Pergamon

Journal of the Mechanics and Physics of Solids
49 (2001) 231–259

JOURNAL OF THE
MECHANICS AND
PHYSICS OF SOLIDS

www.elsevier.com/locate/jmps

The mode I crack growth resistance of metallic foams

C. Chen, N.A. Fleck *, T.J. Lu

Cambridge University Engineering Department, Trumpington Street, Cambridge CP2 1PZ, UK

Received 17 December 1999; received in revised form 19 May 2000

Abstract

A Dugdale-type cohesive zone model is used to predict the mode I crack growth resistance (*R*-curve) of metallic foams, with the fracture process characterised by an idealised traction-separation law that relates the crack surface traction to crack opening displacement. A quadratic yield function, involving the von Mises effective stress and mean stress, is used to account for the plastic compressibility of metallic foams. Finite element calculations are performed for the crack growth resistance under small scale yielding and small scale bridging in plane strain, with K-field boundary conditions. The following effects upon the fracture process are quantified: material hardening, bridging strength, *T*-stress (the non-singular stress acting parallel to the crack plane), and the shape of yield surface. To study the failure behaviour and notch sensitivity of metallic foams in the presence of large scale yielding, a study is made for panels embedded with either a centre-crack or an open hole and subjected to tensile stressing. For the centre-cracked panel, a transition crack size is predicted for which the fracture response switches from net section yielding to elastic-brittle fracture. Likewise, for a panel containing a centre-hole, a transition hole diameter exists for which the fracture response switches from net section yielding to a local maximum stress criterion at the edge of the hole.

Keywords: A. Crack tip plasticity; Notch behaviour; B. Foam material; C. Finite elements

1. Introduction

With recent advances in manufacturing technology, metallic foams with attractive mechanical, thermal and acoustic properties are now available for commercial exploi-

* Corresponding author. Fax.: +44-0122-765046.
E-mail address: naf1@eng.cam.ac.uk (N.A. Fleck).

0022-5096/01/$ - see front matter
PII: S0022-5096(00)00039-9

tation. Potential applications range from energy absorbing components in sandwich structures to compact heat exchangers in novel high power electronic packages (Ashby et al., 2000). Inevitably, as is the case for any new class of engineering materials, the successful application of metallic foams demands a mature level of fundamental understanding of their mechanical properties. A detailed and updated review on these subjects can be found in Gibson and Ashby (1997) and Ashby et al. (2000).

The focus of the present investigation is the application of the cohesive zone model to predict the crack growth initiation and resistance curves of metal foams from pre-existing cracks and holes. A few preliminary remarks on the use of crack-bridging models in non-linear fracture mechanics analysis are appropriate, in order to place this paper in context. For brittle elastic materials, the initiation of crack growth is governed by Griffith's energy release rate criterion $G=G_C$, or, equivalently, by the critical stress intensity factor criterion $K=K_C$. For ductile materials under even small-scale yielding (SSY), however, it is found that the critical energy release rate G_C and the fracture toughness K_C increases with crack extension (i.e. the *R*-curve phenomenon), due to non-proportional stressing within the plastic zone at the crack tip. Much effort has been spent in uncovering the physical basis of the observed *R*-curve phenomenon and to quantify the dependence of total work of fracture on the work of crack separation and crack tip plasticity (see, for instance, Rice and Sorensen, 1978; Tvergaard and Hutchinson, 1992). It has also been recognised that the degree of plastic constraint in large scale yielding affects the crack growth resistance in ductile solids. Therefore, a single loading parameter (such as the *J*-integral) may be inadequate to characterise the fracture response. Although additional parameters such as the *T*-stress (Larsson and Carlsson, 1973; Rice, 1974; Du and Hancock, 1991) and the *Q*-stress (O'Dowd and Shih, 1991) have been introduced to complement the *J*-integral (or the stress intensity factor *K*), further effort is needed to develop a more rigorous account of crack tip constraint effects in the presence of SSY or general yielding (Yuan and Brocks, 1998).

Following Needleman (1987) and the earlier works of Dugdale (1960) and Cottrell (1963), a cohesive zone model embedded in a von Mises solid was used by Tvergaard and Hutchinson (1992) to study the role of plasticity in Mode I crack initiation and growth under the condition of SSY in plane strain. The cohesive zone model is specified through a crack bridging law, with the peak bridging stress σ_0 and the work of separation per unit area Γ_0 as the primary parameters. The cohesive zone model was later extended to study the effect of crack tip constraint, i.e. the *T*-stress effect, and it was shown that the model is able to capture the observed *T*-stress effect realistically in a von Mises material (Tvergaard and Hutchinson, 1994). These authors conclude that the cohesive zone model has considerable promise as a predictive tool for non-linear fracture mechanics analysis, and is equally applicable in SSY and large-scale yielding situations, for both stationary and growing cracks.

Crack-bridging concepts have been applied by Suo et al. (1992) to calculate the delamination *R*-curves of fibre-reinforced ceramic-matrix composites, and by Soutis et al. (1991) and Bao and Suo (1992) to study the toughness, strength and notch-

ductility of metals, composites and, in fact, *any* material whose fracture process may be characterised by a Dugdale-type bridging law.

1.1. Prediction of toughness and notch behaviour of metal foams

For brittle foams having regular open cells, Maiti et al. (1984) proposed a micromechanics model to express the dependence of the fracture toughness K_{IC} upon the cell size l, cell wall fracture strength σ_{fs}, and relative foam density $\bar{\rho}$, as

$$K_{IC}=0.65\sigma_{fs}(\pi l)^{0.5}\bar{\rho}^{1.5} \tag{1}$$

Chen et al. (1998) applied a strain gradient theory to brittle foams and found that, for regular honeycombs, instead of Eq. (1), one has

$$K_{IC}=0.88\sigma_{fs}(\pi l)^{0.5}\bar{\rho} \tag{2}$$

Whereas no experimental data were reported by Chen et al. (1998) to support Eq. (2), good agreement between the predictions of Eq. (1) and experimental measurements has been reported for rigid polymer foams and reticulated vitreous carbon foams (Brezny and Green, 1989; Maiti et al., 1984).

Sugimura et al. (1997) conducted notched bend tests to investigate the crack growth response of a closed cell aluminium alloy foam (trade name "Alporas"), processed by gas-releasing particle decomposition in the melt. Based upon the observation that closed cell metal foams crack by cell wall thinning/tearing, they assume that the crack advances along the thinned region within a fracture process zone, due to the nucleation, plastic growth and coalescence of voids, resulting in

$$K_S\sim(E_s\sigma_{fs}l)^{0.5}\bar{\rho}^{1.5} \tag{3a}$$

where K_S is the steady-state tearing fracture toughness and E_s is the Young's modulus of cell wall material. An alternative model, emphasising that the tearing toughness is due to the bending rather than stretching of cell edges, has been proposed by Olurin et al. (2001). The steady state toughness K_S follows as

$$K_S\sim(E_s\sigma_{fs}l)^{0.5}\bar{\rho}^{1.75} \tag{3b}$$

which is in close agreement with Eq. (3a), except for the slightly greater exponent of $\bar{\rho}$. The recent experiments by McCullough et al. (1999a) and Olurin et al. (2001) on measurement of R-curves for Alulight, Alcan and Alporas aluminium foams support Eq. (3b) in preference to Eq. (3a). A pronounced R-curve was observed due to bridging tractions in the crack wake.

It is of obvious engineering importance to measure and to predict the effect of sharp notches and holes upon the tensile and compressive fracture strengths of metallic foams. Initial studies reveal that foams are relatively notch-insensitive in compression, for both sharp notches and holes: the net section strength is approximately equal to the unnotched strength (McCullough et al., 1999a; Fleck et al., 2001). A complication arises when the net section extends over only a small number of cell sizes, as explored by Sugimura et al. (1997); under these circumstances, they found that the peak compressive strength increases with diminishing net section size. To

date, studies on the tensile fracture of notched specimens have been limited to laboratory-sized specimens (of specimen width less than 500 mm), and the net section strength criterion is obeyed for both centre-hole and centre-crack geometries (Fleck et al., 2001; Ashby et al., 2000). However, metallic foams have a low toughness and it is fully expected that the failure mode in tension, for sharp notches and holes, switches from a predicted net section yielding mode to a brittle mode at sufficiently large specimen sizes. Similar ductile-brittle transitions have been predicted by Bao and Zok (1993) and Suo et al. (1993a) for ductile particle-reinforced elastic materials and fibre-reinforced ceramic matrix composites under tensile stressing by using idealised crack-bridging laws, and by Soutis et al. (1991) for compression loaded carbon fibre/epoxy composite laminates with a Dugdale-type cohesive zone model.

The aim of the present study is to employ a cohesive zone analysis in order to predict the dependence of tensile failure strength upon notch size, for both sharp notches and holes. The linear softening bridging law shown in Fig. 1 is introduced to model the fracture process; other types of bridging law may also be used, but it has already been established that the fracture toughness is dictated by the peak bridging stress σ_0 and the work of separation per unit area Γ_0, but not the shape of bridging curve (Tvergaard and Hutchinson 1992, 1994; Bao and Suo, 1992; Suo et al., 1993a). A phenomenological approach will be adopted here: the heterogeneous metallic foam is replaced by a compressible elastic–plastic power-law hardening solid, with an independently validated elliptical yield surface in von Mises stress versus mean stress space. For metal foam specimens containing either a centre-crack or an open hole subjected to uniaxial tension, the effects of material and geometrical parameters on their tensile strengths are examined and the mechanisms underlying the brittle-ductile transition are explored. In addition, the crack growth resistance curve (*R*-curve) for a semi-infinite crack in SSY is determined to remove the effect of specimen geometry in the long crack limit.

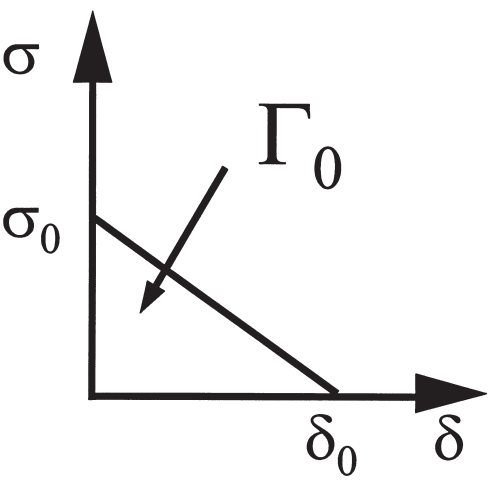

Fig. 1. The traction-separation relation — linear softening bridging law.

2. Problem formulation

2.1. Constitutive model of metallic foams

There have been several attempts to develop constitutive models for ductile foams, mainly to capture the dependence of yielding of these materials on hydrostatic pressure, with varying degrees of success (Gibson et al., 1989; Zhang et al., 1997; Miller, 2000). Recently, based on detailed multi-axial testing data, Deshpande and Fleck (2000) developed a phenomenological constitutive model for both open and closed cell metallic foams (of relative density less than 0.3) under proportional and nearly proportional loadings. Due to its simplicity, the self-similar yield surface model of Deshpande and Fleck (2000) is used in this paper, in conjunction with the method of finite elements, to characterise the constitutive behaviour of metallic foams.

In the self-similar yield surface model, the yield function Φ is assumed to be

$$\Phi=\hat{\sigma}-Y=0 \tag{4}$$

where Y is the uniaxial yield strength and $\hat{\sigma}$ is the effective stress, defined by

$$\hat{\sigma}^2=\frac{1}{1+(\alpha/3)^2}(\sigma_e^2+\alpha^2\sigma_m^2) \tag{5}$$

Here, α defines the aspect ratio of the elliptical yield surface in von Mises stress σ_e versus mean stress σ_m space. Note that for the case $\alpha=0$, the effective stress $\hat{\sigma}$ reduces to σ_e and J_2-flow theory is recovered. Deshpande and Fleck (2000) show that α is related to the plastic Poisson's ν^p ratio by

$$\alpha=3\left(\frac{1/2-\nu^p}{1+\nu^p}\right)^{1/2} \tag{6}$$

Consequently, instead of probing the shape of the initial yield surface and its subsequent evolution from complicated multi-axial tests, it appears from Eq. (6) that the yield surface can be estimated by simply measuring ν^p in a uniaxial test. For Alporas foams of relative density $\bar{\rho}\approx 0.08$, the plastic Poisson's ratio is approximately zero and hence, from Eq. (6), $\alpha\approx 2.12$ (Deshpande and Fleck, 2000).

For simplicity, isotropic hardening is assumed below, i.e. the yield surface grows in a geometrically self-similar manner with strain. This is supported by limited data on the yield surface of Alporas foams (Deshpande and Fleck, 2000). To model the post-yield behaviour, an effective plastic strain rate $\dot{\hat{\varepsilon}}^2$, which is the work rate conjugate to $\hat{\sigma}$, is introduced as

$$\begin{aligned}&\dot{\hat{\varepsilon}}^2=[1+(\alpha/3)^2](\dot{\varepsilon}_e^2+\dot{\varepsilon}_m^2/\alpha^2)\\&\dot{\varepsilon}_e^2=(2/3)\dot{\varepsilon}_{ij}^p\dot{\varepsilon}_{ij}^p, \qquad \dot{\varepsilon}_m=\dot{\varepsilon}_{ii}^p\end{aligned} \tag{7}$$

Here, $\dot{\varepsilon}_{ij}^p$ is the plastic strain rate, $i,j=1,2,3$, and the summation convention over repeated indices applies. With the additional assumption of normality, the plastic strain-rate is given by

$$\dot{\varepsilon}_{ij}^{p}=\dot{\hat{\varepsilon}}\frac{\partial\Phi}{\partial\sigma_{ij}}=\frac{\dot{\hat{\varepsilon}}}{1+(\alpha/3)^2}\left(\frac{3}{2}\frac{s_{ij}}{\hat{\sigma}}+\frac{\alpha^2}{3}\delta_{ij}\frac{\sigma_m}{\hat{\sigma}}\right) \tag{8}$$

where $s_{ij}=\sigma_{ij}-\sigma_m\delta_{ij}$ is the deviatoric stress, δ_{ij} is the Kronecker delta, and the effective strain rate is connected to the effective stress rate by

$$\dot{\hat{\varepsilon}}=\frac{\dot{\hat{\sigma}}}{H(\hat{\sigma})} \tag{9}$$

Here, $H(\hat{\sigma})$ is the tangent of the uniaxial true stress versus logarithmic plastic strain curve at the stress level $\sigma=\hat{\sigma}$.

Except for the shape parameter α to be determined from experiment, the self-similar yield surface model by Deshpande and Fleck (2000) can be defined solely by a uniaxial stress-strain curve which, in the present study, is assumed to have the form

$$\varepsilon=\begin{cases}\sigma/E, & \sigma\le\sigma_y\\ \varepsilon_y(\sigma/\sigma_y)^{1/N}, & \sigma>\sigma_y\end{cases} \tag{10}$$

where E is the Young's modulus, σ_y and ε_y are the initial yield stress and strain, respectively, and N is the strain hardening exponent of the foam. Throughout this paper, unless otherwise stated, the yield strain $\varepsilon_y=0.3\%$ and Poisson's ratio $\nu=0.3$ are used; Tvergaard and Hutchinson (1992) found, at least for von Mises solids, that $\varepsilon_y\equiv\sigma_y/E$ plays an insignificant role in crack growth initiation and resistance. Two typical uniaxial stress-strain curves are shown in Fig. 2a: the choices $N=0.1$ and 0.3 represent foams with weak and strong hardening, respectively. A direct comparison of measured and fitted stress-strain curve is given in Fig. 2b for an Inco nickel foam of relative density 4.3%; in this case, a curve-fit to the data gives $N=0.13$, $E=0.271$ GPa, and $\sigma_y=0.81$ MPa.

2.2. Crack-bridging law

In order to predict the R-curve behaviour and notch sensitivity of any solid, the fracture process must be clearly defined. Two alternative models — the cohesive zone model (Needleman, 1987; Tvergaard and Hutchinson, 1992) and the dislocation-free model (Suo et al., 1993b) — may be used. However, since metallic foams are in the main ductile, the cohesive zone model appears to be more appropriate and is applied in the present study. The cohesive zone model is specified by a crack-bridging law which relates the crack surface traction to crack separation displacement. For Alulight foams, McCullough et al. (1999a) clearly show, aided with scanning electron microscope (SEM) and optical microscope images, that a bridging zone of about four cells in length exists behind the observed crack tip, comprised of torn cell faces and intact cell edges. They also measured the crack-bridging law using deep notched specimens. For tensile stressing, the measured normal traction σ versus crack opening displacement δ resembles that of the linear softening law of Fig. 1 adopted in the present study. For such a bridging law, the work of separation per unit area Γ_0 is given by

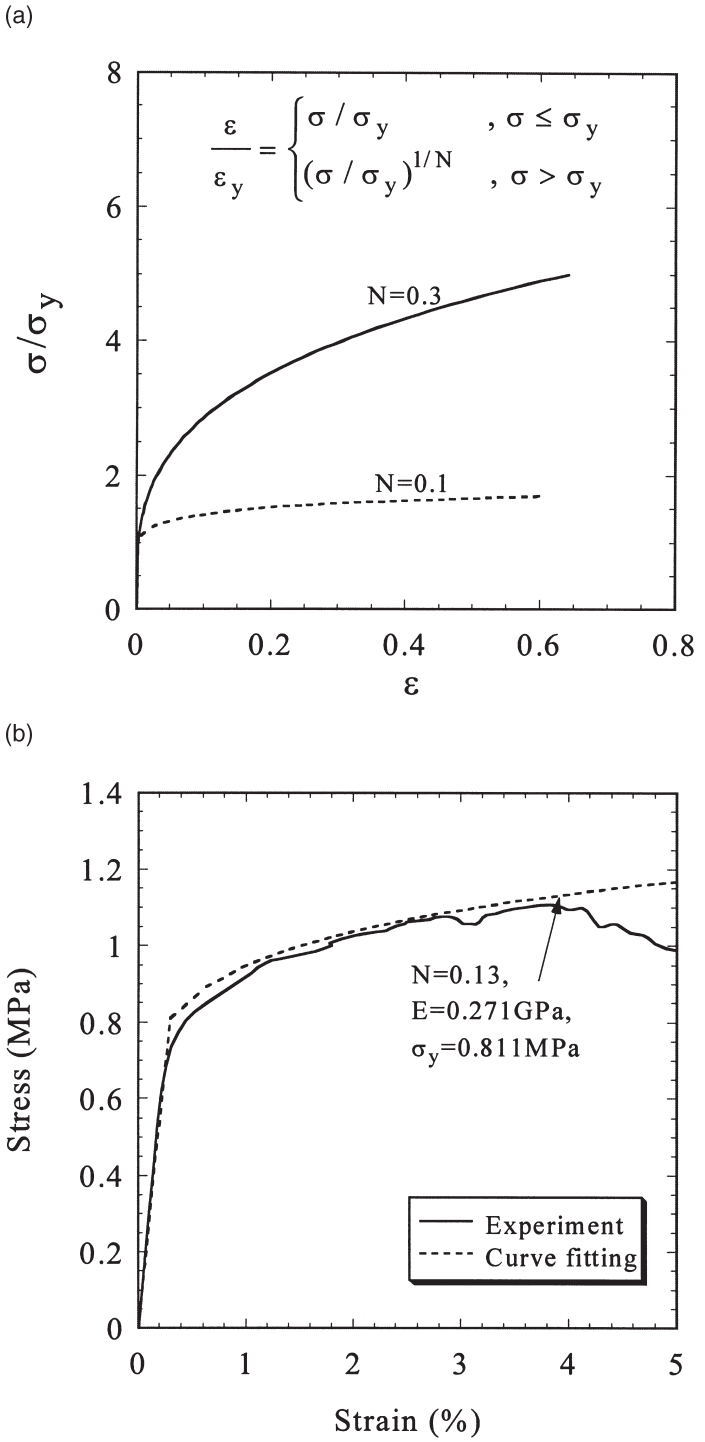

Fig. 2. (a) The uniaxial stress-strain curves used to specify the elasto-plastic behaviour of metallic foams, with ε_y=0.003; (b) Measured and fitted uniaxial tensile stress–strain curves for a Inco nickel foam with a relative density 4.3%, showing the material parameters identified from the measurement.

$$\Gamma_0 = \int_0^{\delta_0} \sigma d\delta = \frac{1}{2}\sigma_0\delta_0 \tag{11}$$

where σ_0 is the peak bridging stress and δ_0 is the critical crack opening displacement. The energy Γ_0 characterises the mode I crack initiation toughness — once the *J*-integral attains the value Γ_0 the crack starts to advance. Although the traction versus separation relation may have other forms, such as linear hardening and rectilinear laws, it has already been established (Tvergaard and Hutchinson 1992, 1994; Bao and Suo, 1992; Suo et al., 1993a) that the shape of the crack-bridging law plays only a minor role in the modelling of the fracture process: Γ_0 and σ_0 are the controlling parameters.

For Alulight foams, McCullough et al. (1999a) found that σ_0/σ_y=1~1.5 depending on the foam relative density $\bar{\rho}$, with σ_0/σ_y decreasing as $\bar{\rho}$ is increased. They also measured the initiation toughness Γ_0 as

$$\Gamma_0 = 10\bar{\rho}^{1.6}\ (\mathrm{kJm^{-2}})$$

In a related study, McCullough et al. (1999b) measured the uniaxial stress–strain response behaviours of Alulight, and conclude that these foams are weakly hardening ($N \approx 0.1$) once the applied strain exceeds the initial yield strain ε_y typically in the range of 0.2~0.5%. Similar findings are reported for two other types of aluminium alloy foam, Alporas and Alcan (Sugimura et al., 1997; Olurin et al., 2001).

3. Finite element model

3.1. Crack growth initiation and resistance in SSY

The self-similar yield surface model, as summarised in Eqs. (4)–(9), has been implemented in a commercial finite element code (ABAQUS, 1997) via a user subroutine (Chen, 1998). To study the initiation and subsequent growth resistance of a mode I crack in metallic foams, the assumptions of small scale yielding and plane strain are made, following the work of Tvergaard and Hutchinson (1992, 1994) for a von Mises solid. Due to symmetry, finite element calculations are only carried out for a semi-circular region of radius *R* (Fig. 3a), with four-node isoparametric elements used throughout. A Cartesian co-ordinate system x_1–x_2 is chosen such that its origin is placed at the initial crack tip and the x_1-axis lies along the crack plane. Since mode I crack growth is of concern, the crack is confined to advance in the positive direction of the *x*-axis. A thin uniform region surrounding the initial crack tip, containing approximately square elements of size Δ, is used to model crack growth, with a total length of about 160Δ and a height of about 4Δ (Fig. 3b). For the region shown in Fig. 3, the crack bridging law is implemented in the finite element model by assigning spring elements everywhere directly ahead of the crack tip on the crack plane, i.e. $x_1 \geq 0$ and $x_2 = 0$; zero traction boundary conditions are enforced on the crack surface, i.e. $x_1 \leq 0$ and $x_2 = 0$.

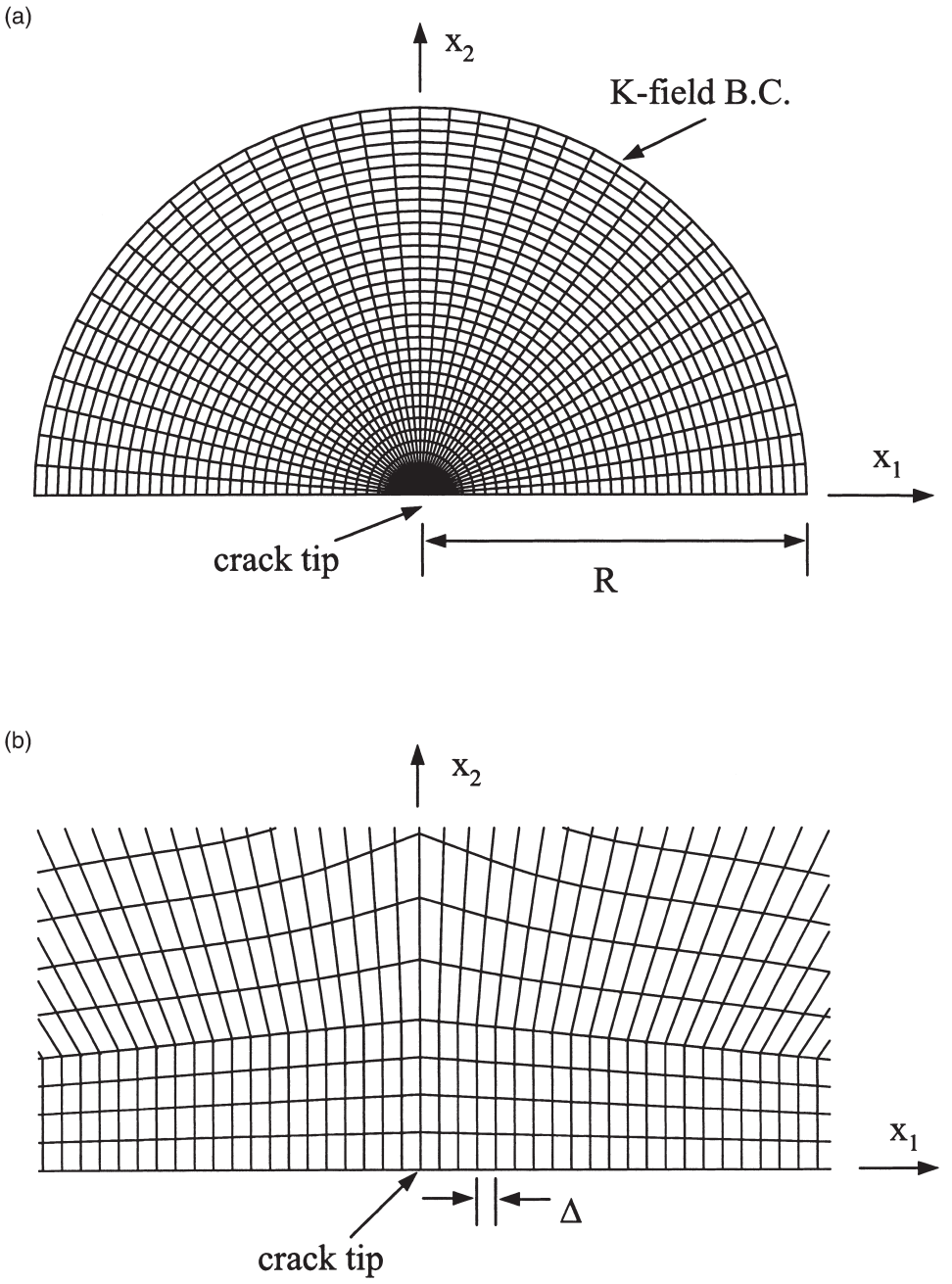

Fig. 3. Typical mesh used in the finite element simulation of small scale yielding with K-field boundary conditions. (a) Full mesh; (b) refined mesh near the crack tip.

Displacement loading is imposed on the outer semi-circular boundary of the mesh in accordance with the *K*-field around the initial crack tip, as

$$u_1 = \frac{K_I}{2\mu}\sqrt{\frac{r}{2\pi}}(3-4\nu-\cos\theta)\cos\frac{\theta}{2} + \frac{(1-\nu)T}{2\mu}r\cos\theta$$
$$u_2 = \frac{K_I}{2}\sqrt{\frac{r}{2\pi}}(3-4\nu-\cos\theta)\sin\frac{\theta}{2} - \frac{\nu T}{2\mu}r\cos\theta \quad (12)$$

where K_I is the mode I stress intensity factor, μ is the shear modulus, (r,θ) are polar co-ordinates centred at the initial crack tip, and T is a non-singular stress acting parallel to the crack plane. The loading is imposed by first increasing the T-stress to the desired level with K_I=0; additional displacements are subsequently specified on r=R according to Eq. (12) by increasing K_I, with T maintained at the pre-set value. Note that, in reality, the values of K_I and T are increased simultaneously on the cracked specimen, whereas in the numerical calculations T is applied first and then held constant. However, as discussed by Tvergaard and Hutchinson (1994), this will not affect the initiation of crack growth at K=K_0 and the toughness of the specimen at steady-state crack growth at K=K_{ss}; only the rising part of the R-curve may be slightly affected.

To ensure that the SSY assumption is satisfied, the finite element mesh must be sufficiently large. A mesh sensitivity study has been carried out and it was established that a finite element mesh with R/Δ =24 000 is sufficient. In addition, the calculated R-curves are found to converge when Δ is less than about four times the critical bridging displacement δ_0. Consequently, in all subsequent calculations, the choices R/Δ=24 000 and Δ/δ_0=2 are used. The details of the numerical scheme follow those of Tvergaard and Hutchinson (1992, 1994). Selected finite element calculations confirm that the present model is able to reproduce the results obtained by Tvergaard and Hutchinson (1992, 1994) for the limiting case of a von Mises elastic-plastic solid.

3.2. Notch sensitivity

The tensile strength and notch sensitivity of metallic foams were studied for specimens containing either a centre-crack (Fig. 4a) or an open hole (Fig. 4b), under remote uniaxial tension σ^∞. For specimens containing a centre-crack, the crack length and specimen width are denoted by 2a and 2w, respectively. Similarly, for specimens containing an open hole, D and W denote the hole diameter and specimen width, respectively. In the numerical calculations, the specimen length L is chosen such that $L>>2w$ and $L>>W$. To model crack growth, spring elements satisfying the linear softening bridging law of Fig. 1 are assigned everywhere along the dashed lines in Fig. 4. Due to symmetry, only a quarter of each specimen is discretised and analysed.

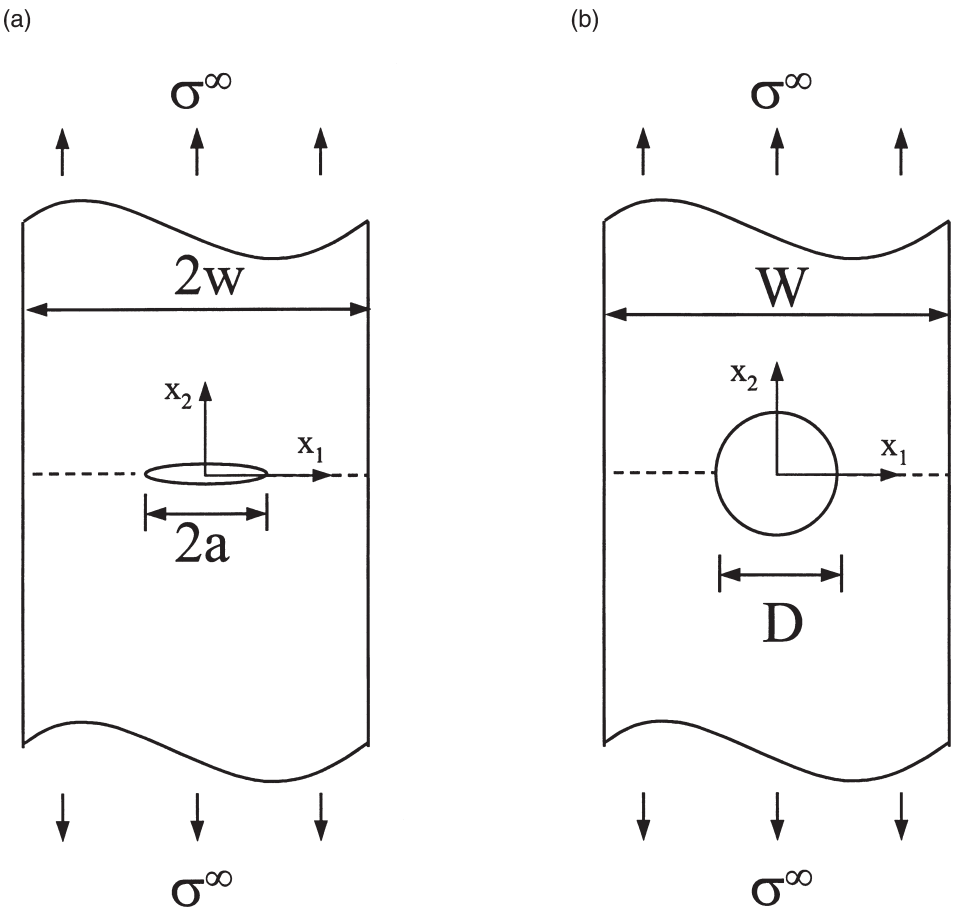

Fig. 4. Specimen with (a) centre-crack and (b) centre-hole.

4. Results and discussion

4.1. Crack tip plastic zone in small scale yielding (SSY)

We begin by quantifying the effect of the yield surface shape (as parameterised by α) upon the shape and size of the plastic zone surrounding the tip of a stationary crack under SSY and plane strain conditions.

A rough estimate of the plastic zone boundary is made by neglecting the stress relaxation due to plastic deformation. According to Westergaard's asymptotic elastic solution, the mode I stress field in polar co-ordinates has the form,

$$\sigma_{11}=\frac{K_I}{\sqrt{2\pi r}}\cos\frac{\theta}{2}\left(1-\sin\frac{\theta}{2}\sin\frac{3\theta}{2}\right)+T,\quad \sigma_{22}=\frac{K_I}{\sqrt{2\pi r}}\cos\frac{\theta}{2}\left(1+\sin\frac{\theta}{2}\sin\frac{3\theta}{2}\right)$$
$$\sigma_{12}=\frac{K_I}{\sqrt{2\pi r}}\cos\frac{\theta}{2}\sin\frac{\theta}{2}\cos\frac{3\theta}{2},\qquad \sigma_{33}=\nu(\sigma_{11}+\sigma_{22}) \tag{13}$$

The out-of-plane shear stresses are zero. Upon substituting the elastic K-field solution Eq. (13) into the yield criterion Eq. (4), the boundary of the plastic zone $r_p(\theta)$ can be calculated. For the limiting case of T=0, $r_p(\theta)$, has a fairly simple expression, given by

$$r_p=\frac{K_I^2\cos^2\frac{\theta}{2}}{2\pi(9+\alpha^2)\sigma_y^2}\left[9(1-2\nu)^2+4\alpha^2(1+\nu)^2+27\sin^2\frac{\theta}{2}\right] \tag{14}$$

Conventionally, the plastic zone size r_{p0} is defined by

$$r_{p0}=r_p|_{\theta=0} \tag{15}$$

which, for the T=0 case, is

$$r_{p0}=\frac{K_I^2}{2\pi(9+\alpha^2)\sigma_y^2}[9(1-2\nu)^2+4\alpha^2(1+\nu)^2] \tag{16}$$

We emphasise that the above estimate of the plastic zone boundary is based on the elastic solution and ignores the effect of stress re-distribution within the plastic zone. A more accurate estimate of $r_p(\theta)$ has been obtained by using the finite element method. The same finite element model as shown in Fig. 2 is employed, except that the displacement component u_2 of every node along the potential crack line, x_2=0 and $x_1\geq 0$, is now held at zero, and the spring elements have been removed. Moreover, the hardening index N in Eq. (10) is taken to be zero to represent the elastic-perfectly plastic case. The dependence of plastic zone size r_{p0} on α is shown in Fig. 5 for selected values of the T-stress, where the results have been normalised by the plane-strain plastic zone size in a von Mises solid r_0 (Irwin, 1957)

$$r_0=\frac{1}{3\pi}\left(\frac{K_I}{\sigma_y}\right)^2 \tag{17}$$

The predictions of r_{p0}, both from Eq. (16) and from the finite element calculations, are displayed in Fig. 5. It is seen that Eq. (16) slightly underestimates r_{p0} if $T\leq 0$ and slightly overestimates r_{p0} if $T>0$, with the discrepancy between the analytical and numerical predictions increasing as the aspect ratio of the yield surface α increases. The plastic zone size r_{p0} increases with increasing α, and is particularly sensitive to the value of α when $T>0$. This is consistent with the notion that mean stress promotes yield for increasing value of α. According to Deshpande and Fleck (2000), α ranges from 1.35 to 2.12 for typical aluminium alloy foams. Consequently,

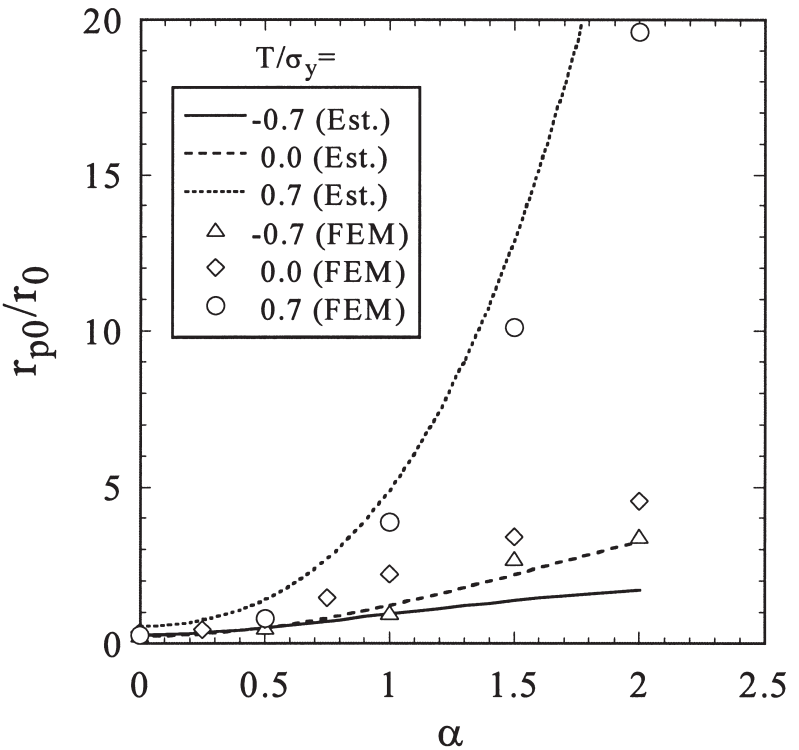

Fig. 5. Effect of α on the plastic zone size of a plane strain mode I crack in metallic foams with ν=0.3 and N=0. Lines represent analytical results, and symbols denote finite element results.

the plastic zone size of a metallic foams may be an order of magnitude larger than that for a von Mises material (α=0) at a fixed level of K_I.

The plastic zone boundaries calculated from the finite element method are plotted in Fig. 6 for selected values of α with T=0, and in Fig. 7 for selected values of T-stress with, α=0, α=1, and α=2. (Although not shown explicitly for the sake of brevity, it has been established that the analytical prediction, such as Eq. (14) for the T=0 case, qualitatively captures the shape of the plastic zone boundary.) It is seen from Fig. 6 that, for the case of T=0, the plastic zone expands as α increases in value, with the expansion in the x_1 direction more significant than that in the x_2 direction — the resulting plastic zones for $\alpha>1$ resemble the shape of a plane-stress plastic zone in a von Mises solid.

For the plastically incompressible solid (α=0), the plastic zone is enlarged significantly by a negative T-stress term and slightly by a positive T-stress term, even though the plastic zone size as defined by Eq. (15) barely change in both cases (Fig. 7a). This observation partially explains why the fracture toughness of fully dense metals is significantly larger in the presence of negative T-stresses and insensitive to positive T-stresses, Tvergaard and Hutchinson (1994). For a plastically compressible material with α=1, both positive and negative T-stress terms increase significantly

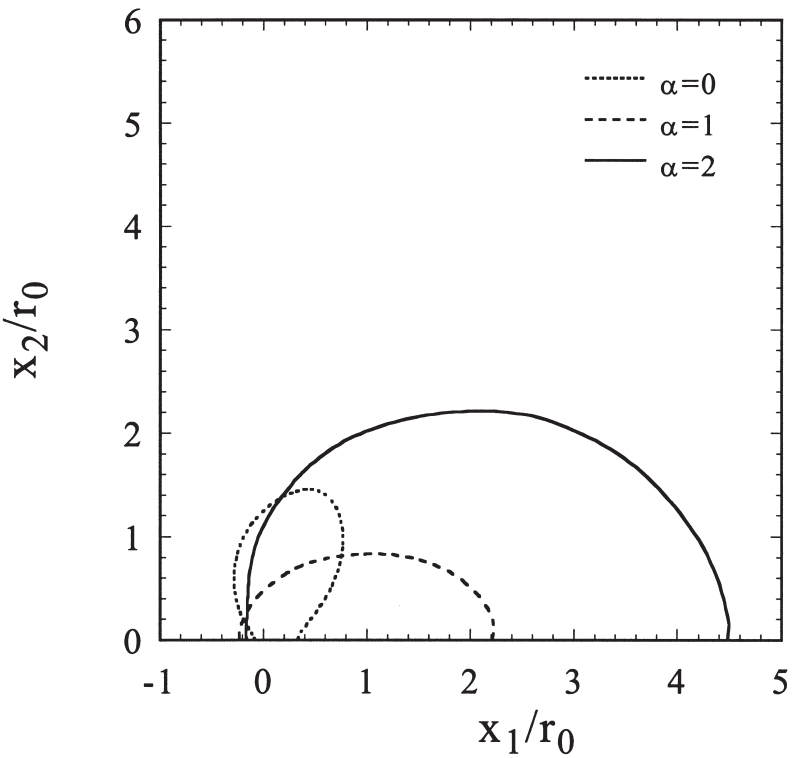

Fig. 6. Effect of α on the plastic zone shape around the plane strain mode I crack tip with $T/\sigma_y=0$, $\nu=0.3$ and $N=0$.

the plastic zone size (Fig. 7b). Furthermore, negative T-stresses tilt the plastic zone forward whereas positive T-stresses rotate the plastic zone backwards, see Figs. 7a and b. For metal foams with $\alpha=2$, the plastic zone increases in an almost self-similar manner with the level of T-stress (Fig. 7c); the plastic zone is enlarged significantly by positive T-stresses and is slightly reduced by negative T-stresses, in sharp contrast to the trends shown in Figs. 7a and b for the $\alpha=0$ and $\alpha=1$ cases.

4.2. Crack growth initiation

Under SSY, metallic foams are observed to display a typical R-curve behaviour — crack growth initiates at $K=K_0$, and subsequent growth requires an increasing K until a steady-state value K_{SS} is attained (McCullough et al., 1999a; Olurin et al., 2001). In this section, the cohesive zone model is used to predict R-curves for metallic foams. We begin by introducing two reference quantities K_0 and R_0,

$$K_0=\left(\frac{E\Gamma_0}{1-\nu^2}\right)^{1/2},\ R_0=\frac{1}{3\pi}\left(\frac{K_0}{\sigma_y}\right)^2 \tag{18}$$

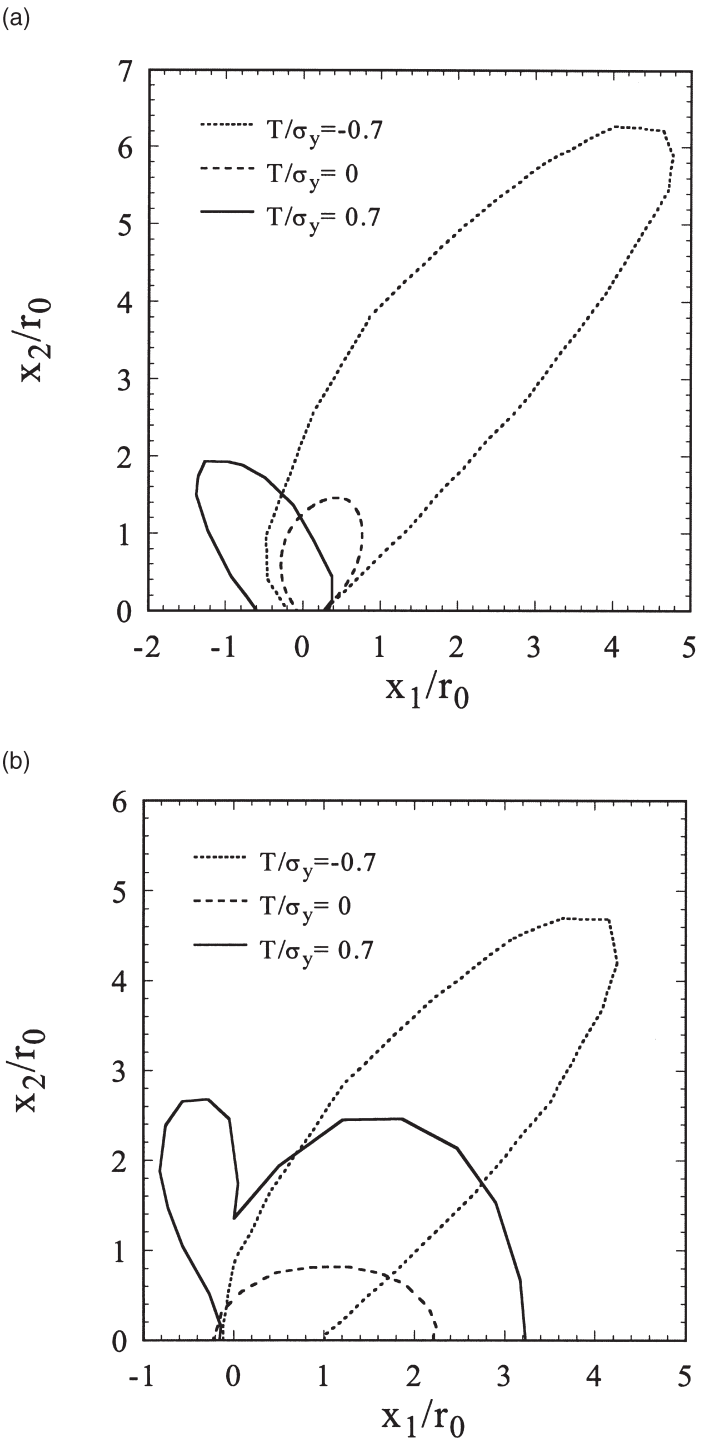

Fig. 7. Effect of *T*-stress on the plastic zone shape around the plane strain mode I crack tip with ν=0.3 and N=0. (a) α=0; (b) α=1; (c) α=2.

(c)

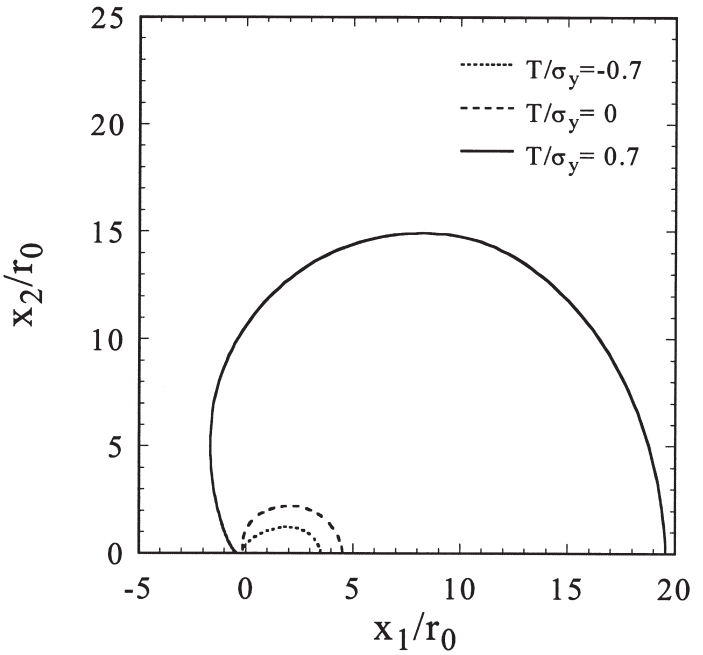

Fig. 7. (*continued*)

Note that R_0 is the size of the Irwin plane-strain plastic zone corresponding to a load level of $K=K_0$. The crack growth resistance curve can then be expressed as

$$\frac{K_R}{K_0}=1+f\left(\frac{\Delta a}{R_0},\frac{\sigma_0}{\sigma_y},N,\alpha,T\right) \tag{19}$$

where Δa represents the amount of crack extension at $K=K_R$; the dimensionless function f accounts for the extra contribution of plasticity to crack growth resistance, with $f\geq 0$ expected for all values of Δa. As previously discussed, the effects of Poisson's ratio ν and yield strain ε_y are small, and can be neglected in Eq. (19).

Fig. 8 displays the normalised crack growth resistance K_R/K_0 as a function of normalised crack extension $\Delta a/R_0$ for the case (N=0.1, σ_0/σ_y=1.6), with three levels of T-stress:, $T/\sigma_y = -1$, 0, 1. Two values of α (i.e. α=1 and 2) are considered, representing foams with low and high compressibility, respectively. It is seen that the mode I crack experiences a rapidly increasing resistance to growth over small values of $\Delta a/R_0$; with further growth, the additional resistance to growth diminishes until a steady-state of crack growth is reached. Consider first the case α=1. A positive T-stress of T/σ_y=1 increases the resistance K_R by less than 10%, whereas a negative T-stress of $T/\sigma_y= -1$ nearly doubles the asymptotic steady-state value K_{SS}. Thus, for solids of low compressibility (e.g. α=1), the T-stress effect upon crack growth is similar to that reported in Tvergaard and Hutchinson (1994) for a von Mises solid.

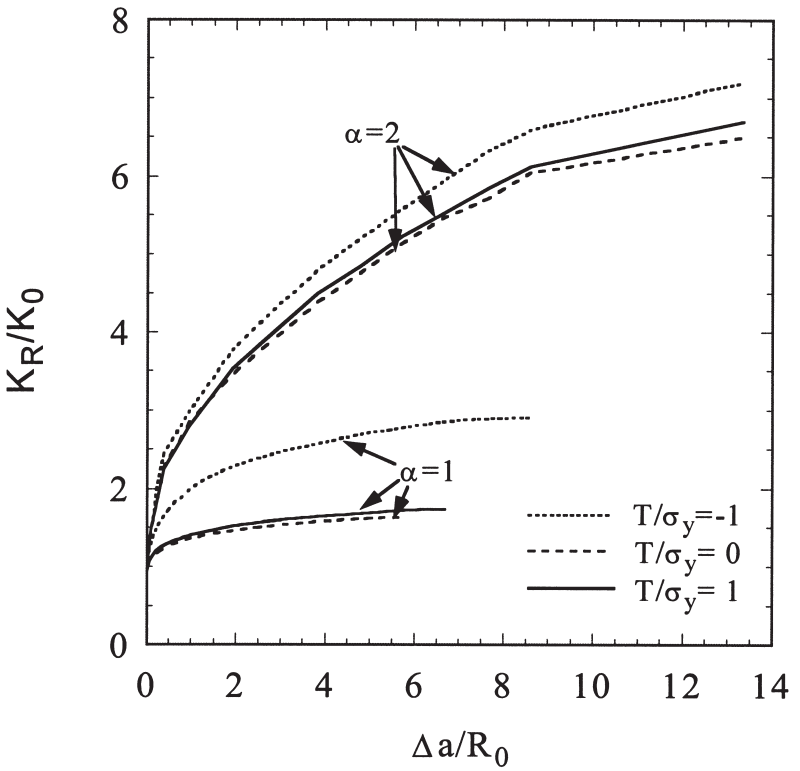

Fig. 8. Effect of T-stress on the calculated R curves of metallic foams with N=0.1, ν=0.3 and σ_0/σ_y=1.6.

This may be explained by the reduction of crack-tip constraint due to negative T-stresses and the relatively high crack-tip constraint that is sustained in the presence of positive T-stresses (Du and Hancock, 1991; Tvergaard and Hutchinson, 1994). The presence of a negative T-stress reduces the tensile stress level in front of the crack-tip; thus, an increased value of K is required to break the crack-bridging elements than that needed for the case $T>0$. However, in all cases, crack initiation starts at $K=K_0$, independent of both α and T, a fact which is reflected in Eq. (19). Next, consider the R-curve for the case α=2, as summarised in Fig. 8; the crack growth resistance curve is relatively insensitive to the value of T-stress, in contrast to the case α=1. We conclude that the T-stress effect on the R-curve diminishes with increasing plastic compressibility of the foam. Typically, metallic foams have an α-value of about 2, and so the above analysis suggests that specimen geometry (with attendant differences in T-stress level) has only a minor effect upon the measured R-curve.

The dependence of crack growth resistance on peak bridging stress σ_0/σ_y is presented in Fig. 9 for a metallic foam with α=2, N=0.1 and T/σ_y=0. When $\sigma_0/\sigma_y \leq 1.5$, the metallic foam has essentially a flat K_R curve with little toughness enhancement from plasticity. However, a slight increase of σ_0/σ_y from σ_0/σ_y=1.5 to

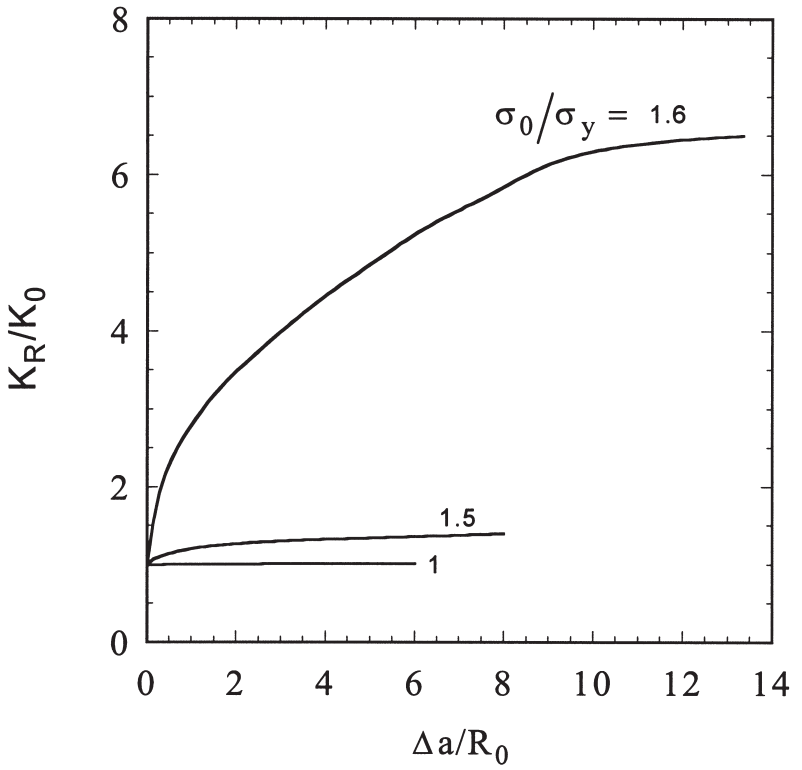

Fig. 9. Effect of the bridging strength on the calculated R curves of metallic foams with α=2, ν=0.3, T/σ_y=0 and N=0.1.

1.6 leads to a pronounced *R*-curve. We conclude that the peak bridging stress σ_0 plays a vital role in determining the crack growth resistance for metallic foams. If the peak bridging stress σ_0 is smaller than a critical value, then little or no crack growth resistance beyond the initiation toughness is expected, whereas significant crack growth resistance is present once σ_0 exceeds the critical value.

4.3. Steady-state crack growth

We will use the steady-state crack growth resistance K_{SS} to denote the fracture toughness of metallic foams, with

$$\frac{K_{SS}}{K_0}=1+f\left(\frac{\sigma_0}{\sigma_y},\frac{T}{\sigma_y},N,\alpha\right) \tag{20}$$

Figs. 10a and b display the ratio K_{SS}/K_0 as a function of the normalised bridging strength σ_0/σ_y, for α=1 and 2, respectively. For reference, Fig. 10b includes the numerical results of Tvergaard and Hutchinson (1992) for the von Mises solid (α=0, N=0.1). Recall that K_{SS} has a negligible dependence upon the level of *T*-stress when

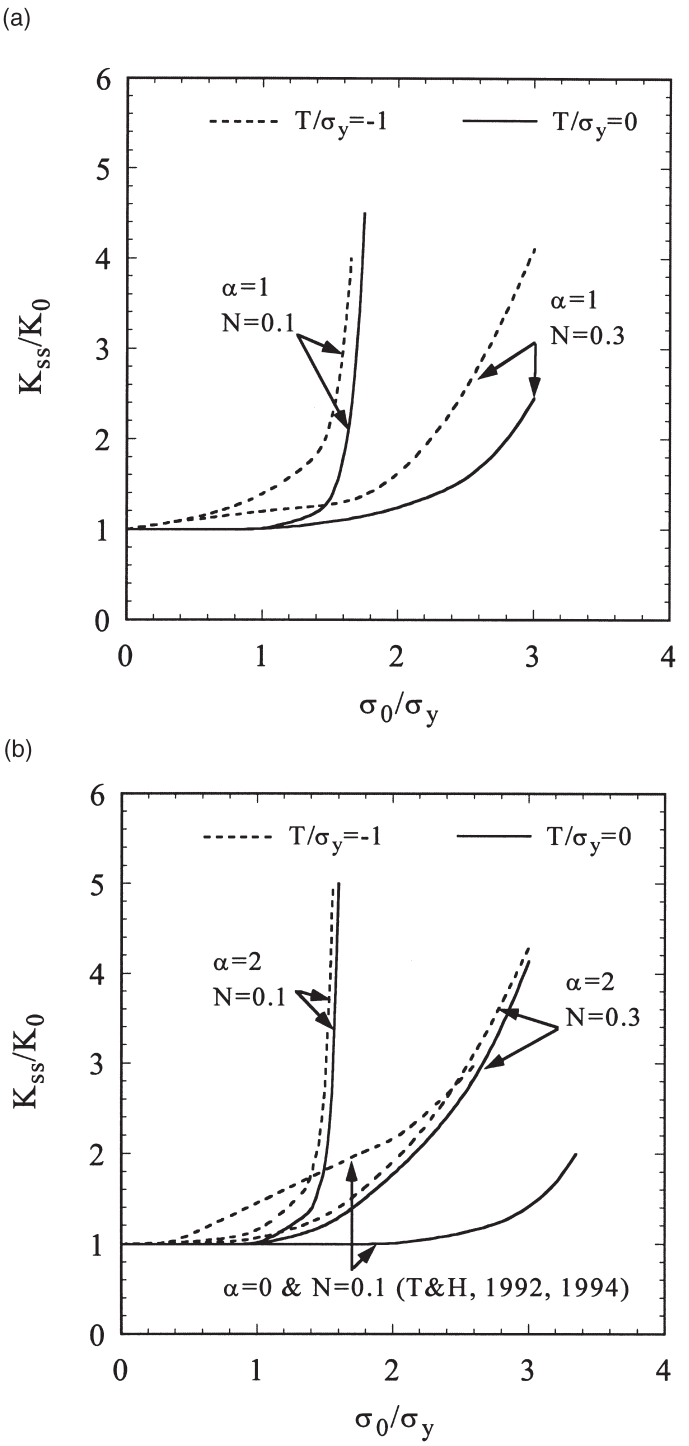

Fig. 10. The dependence of the steady state toughness on the bridging strength of metallic foams. (a) α=1; (b) α=2.

$T \geq 0$, for all values of α considered. Consequently, results have been omitted for the case of positive T-stress. It is clear from Figs. 10a and b that the presence of a negative T-stress has a minor effect upon K_{SS}/K_0 for $\alpha=1$, and has a negligible effect upon K_{SS}/K_0 for $\alpha=2$.

Consider further the steady-state crack growth resistance K_{SS} of metallic foams (for which $\alpha>0$), for the case of vanishing T- stress. It is seen from both Figs. 10a and b that K_{SS} is only slightly larger than the initiation value K_0 provided the bridging strength σ_0 is less than the material yield strength σ_y. This can be explained as follows. Additional finite element calculations have been performed for the SSY problem of the non-hardening metallic foam ($N=0$), with the cohesive zone suppressed in order to assess the stress level ahead of the crack tip. The tensile stress acting normal to the crack plane immediately ahead of the crack tip is about $\sigma_{22} \approx 1.3\sigma_y$ for $\alpha=1$ and is about $\sigma_{22} \approx \sigma_y$ for $\alpha=2$; the corresponding crack-tip stress for an elastic-ideally plastic von Mises solid is about $\sigma_{22} \approx 3\sigma_y$. Consequently, if the metallic foam has a bridging strength less than about $1.3\sigma_y$, the crack will initiate and advance without a fully developed plastic zone. Under such conditions, the contribution of plasticity to K_{SS} is small.

For weakly hardening foams ($N=0.1$), the abrupt increase in K_{SS}/K_0 at a bridging strength of about $\sigma_0=1.6\sigma_y$ suggests that a tensile traction greater than $1.6\sigma_y$ is hardly attainable ahead of the crack tip although the corresponding tensile traction for a von Mises solid attains a level of $3.5\sigma_y$ or higher (as implied by the results shown in Fig. 10b, and as discussed by Tvergaard and Hutchinson, 1992). An increase in the strain hardening exponent N leads to higher stresses ahead of the tip of a stationary crack in a compressible foam (and for an incompressible solid); consequently, the cut-off value of σ_0/σ_y at which K_{SS}/K_0 rises steeply increases with increasing N.

4.4. Notch sensitivity

To study the notch sensitivity of metallic foams, a panel of finite width containing either a centre-crack (Fig. 4a) or an open hole (Fig. 4b) has been analysed using the cohesive zone model. Both specimens are subjected to remote uniaxial tension σ^∞. The ultimate tensile strength of the specimens is denoted by the peak value σ_{max} of σ^∞. The length scale a_0 is introduced as a reference length for the notch size, where

$$a_0=\frac{E\Gamma_0}{\pi(1-\nu^2)\sigma_0^2}=\frac{1}{\pi}\left(\frac{K_0}{\sigma_0}\right)^2 \tag{21}$$

Consider first the case of a cohesive zone placed across the net section of an *elastic specimen*. Then, the notch brittle-ductile transition behaviour is dictated by the notch and specimen size. Specifically, for the centre-crack specimen, one has a ductile response

$$\frac{\sigma_{max}^{net}}{\sigma_0}=1 \tag{22}$$

in the limit $a/a_0 \to 0$, and a brittle response

$$\frac{\sigma_{\max}^{net}}{\sigma_0}=\left(F^2\frac{a}{a_0}\right)^{-1/2} \tag{23}$$

in the limit $a/a_0\to\infty$. Here, $\sigma_{\max}^{net}$ is the net section strength related to $\sigma_{\max}$ by $\sigma_{\max}^{net}=\sigma_{\max}/(1-a/w)$, and F is the finite width correction factor (Tada et al., 1985)

$$F(a/w)=[1-0.5(a/w)+0.326(a/w)^2] \tag{24}$$

For intermediate values of a/a_0, Suo et al. (1993a) suggest a simple interpolation of the two limiting values given by Eqs. (22) and (23), as

$$\frac{\sigma_{\max}^{net}}{\sigma_0}=\left[1+F^2\frac{a}{a_0}\right]^{-1/2} \tag{25}$$

Similarly, for specimens containing a centre-hole, the notch-ductile limit is given by

$$\frac{\sigma_{\max}^{net}}{\sigma_0}=1, \text{ when } D/a_0\to 0 \tag{26}$$

and the notch-brittle limit by

$$\frac{\sigma_{\max}^{net}}{\sigma_0}=\frac{1}{k_E}, \text{ when } D/a_0\to\infty \tag{27}$$

where $\sigma_{\max}^{net}=\sigma_{\max}/(1-D/W)$ is the net section strength and k_E is the elastic stress concentration factor ($k_E=3$ for a hole embedded in an infinite specimen). The effects of intermediate values of D/a_0 on $\sigma_{\max}^{net}/\sigma_0$ have also been quantified by Suo et al. (1993a) for the cohesive zone model with an elastic matrix.

Now consider the expected response for metallic foams via the cohesive zone model with a *compressible elastic-plastic matrix*. For panels containing cracks or holes, and loaded in remote tension, we expect a notch-brittle behaviour for large notch sizes and a notch-ductile behaviour for small notch sizes. However, the transition from a notch-brittle to a notch-ductile response depends not only upon the notch length and specimen size but also upon the material parameters σ_0/σ_y, N and α. The focus below will be to quantify the effects of these material and geometrical parameters upon the ultimate strength $\sigma_{\max}$. Since metallic foams exhibit a R-curve behaviour, their ultimate tensile strength for large initial crack lengths under small scale yielding is governed by the steady state toughness K_{SS}, instead of by the initial toughness K_0. Consequently, it is appropriate to define another reference length a_{SS} as

$$a_{SS}=\frac{1}{\pi}\left(\frac{K_{SS}}{\sigma_0}\right)^2 \tag{28}$$

The notch-ductile behaviour of centre-crack specimens made of metallic foams at small values of a/a_{SS} is still characterised by Eq. (22), whereas their notch-brittle behaviour at large values of a/a_{SS} is now described by

$$\frac{\sigma_{\max}^{net}}{\sigma_0}=\left(F^2\frac{a}{a_{SS}}\right)^{-1/2},\ \frac{a}{a_{SS}}\rightarrow\infty \tag{29}$$

For intermediate values of a/a_{SS}, an interpolation relation similar to Eq. (25) may be written as

$$\frac{\sigma_{\max}^{net}}{\sigma_0}=\left[1+\left(F^2\frac{a}{a_{SS}}\right)^{m/2}\right]^{-1/m} \tag{30}$$

where m has been introduced as a curve fitting parameter to obtain good agreement between the predictions based on Eq. (30) and the finite element simulations. It is noted that Eq. (30) represents the bi-linear curves Eqs. (22) and (29) in the limit $m\rightarrow\infty$.

For the case of centre-hole specimens made from a *compressible elastic-plastic solid,* the limiting behaviour for a small hole is still given by Eq. (26), derived for an elastic solid. However, the expression Eq. (27) for the strength ratio for a large hole now becomes

$$\frac{\sigma_{\max}^{net}}{\sigma_0}=\frac{1}{k},\ \text{when } D/a_0\rightarrow\infty \tag{31}$$

where the stress concentration factor k equals the elastic value k_E for $\sigma_0/\sigma_y\leq 1$, and approaches the plastic stress concentration factor k_P when $\sigma_0/\sigma_y>>1$. (It is recalled that the plastic stress concentration factor is defined as the ratio of the local maximum stress at the hole edge to the net section stress, when loading is deep in the plastic range.) For the compressible elastic-plastic matrix, the value of k_P depends upon N and α in addition to D/W; in fact, numerical experimentation reveals that k_P is almost independent of α.

Calculations of the tensile strength of centre-crack specimens have been carried out for various values of N, σ_0/σ_y and α, with a/w=0.1. To represent both weak and strong hardening behaviours, the values N=0.1 and 0.3 are chosen, with the bridging strength held fixed at σ_0/σ_y=1.6 and 3, respectively, in order to give K_{SS}/K_0 values of 6.5 and 4.0. The predictions of $\sigma_{\max}^{net}/\sigma_0$ versus a/a_{SS} are presented in Fig. 11, for three values of α (i.e. α=0, 1, and 2), with the finite element results denoted by symbols and the expression Eq. (30) by lines associated with selected values of m. In order to construct Fig. 11, the steady-state fracture toughness K_{SS} in each case is determined from Fig. 10 for the choice T/σ_y=0. As is evident from Fig. 11, the notch-ductile behaviour of metallic foams at small a/a_{SS} values is described fairly accurately by Eq. (22) whilst their notch-brittle behaviour follows closely Eq. (29) at large a/a_{SS} values. For intermediate a/a_{SS}, Eq. (30) gives a good estimate of the transition behaviour, but the optimal value of m depends somewhat upon the material parameters N, σ_0/σ_y and α. For example, m=0.8 is optimal for a foam with N=0.3, σ_0/σ_y=3, and α=3.

The effect of the specimen aspect ratio a/w upon the tensile strength is explored in Fig. 12, for a fixed set of material parameters (N=0.3, σ_0/σ_y=3, α=2). For all a/w considered, the analytical expression Eq. (30) is in good agreement with the finite element predictions for the choice m=0.8.

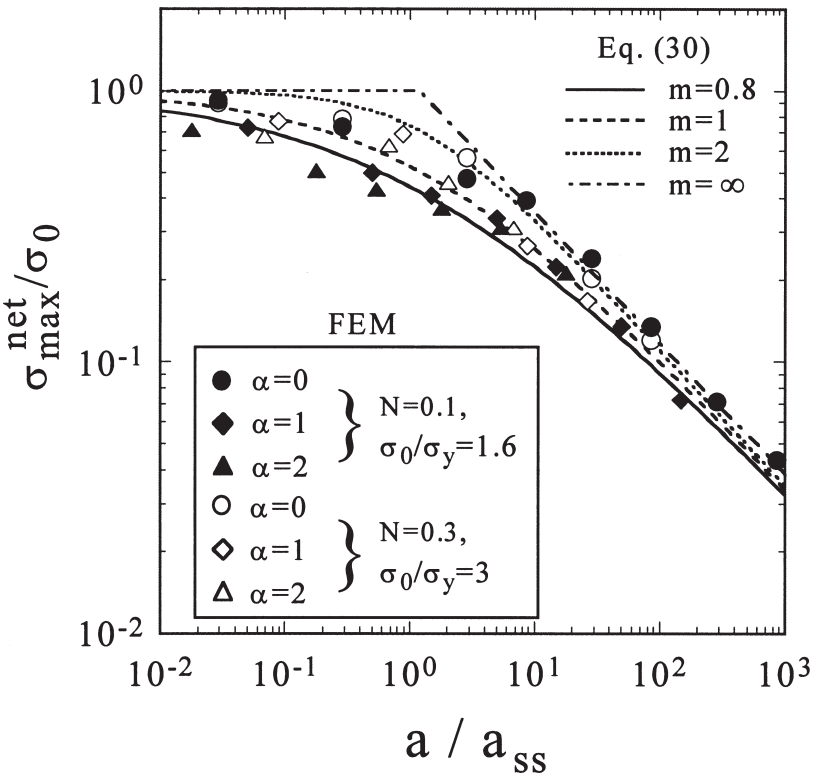

Fig. 11. Effect of the crack length upon the tensile strength of centre-crack specimens made of metallic foams for the case a/w=0.1.

Finite element calculations were also conducted for metal foam panels of width W, containing a centre-hole of diameter D. The predictions for D/W=0.1 are displayed in Fig. 13a–d for selected values of the material parameters, as follows. The effect of α-value upon the net section tensile strength is shown in Fig. 13a for N=0.1, and in Fig. 13b for N=0.3. The effect of the ratio of cohesive strength σ_0 to yield strength σ_y upon the failure strength is summarised in Fig. 13c for N=0.1 and in Fig. 13d for N=0.3. In each figure, the predictions for an elastic matrix are included for comparison. For all cases shown in Fig. 13a–d, the normalised tensile strength $\sigma^{net}_{max}/\sigma_0$ of a central-hole specimen decreases with increasing hole size D/a_0, and approaches a plateau value of $1/k$ when D/a_0 is larger than about unity. As discussed above, the asymptotic value $1/k$ equals the elastic value $1/k_E$ when $\sigma_0/\sigma_y \leq 1$, and equals the plastic value $1/k_P$ when $\sigma_0/\sigma_y >> 1$. For intermediate values of σ_0/σ_y, k is in the range $k_P \leq k \leq k_E$. Values of the elastic stress concentration factor k_E and of the plastic stress concentration factor k_P have been obtained by performing finite element calculations with the cohesive zone absent, and the results are included in Fig. 13a–d.

On taking Figs. 13a and b together, we note that the failure strength is almost insensitive to the degree of plastic compressibility, as parameterised by α. In both

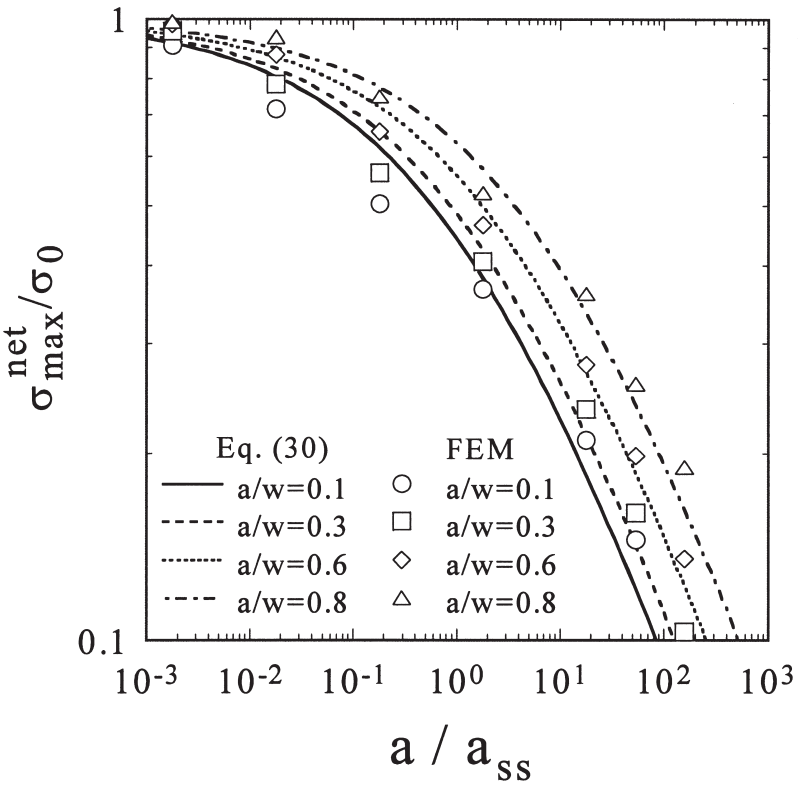

Fig. 12. Effect of the crack length upon the tensile strength of centre-crack specimens made of metallic foams with α=2, N=0.3 and σ_0/σ_y=3. Results are shown for selected values of a/w.

figures, the asymptotic strength ratio at large hole diameter is close to the value $1/k_P$ since the ratio σ_0/σ_y is sufficiently large (σ_0/σ_y=1.6 for N=0.1 and σ_0/σ_y=3.0 for N=0.3). Next, consider the effect of the ratio σ_0/σ_y upon the failure strength, as shown in Fig. 13c for N=0.1 and in Fig. 13d for N=0.3. As σ_0/σ_y increases from unity, the asymptotic strength at large D increases from the lower limit $1/k_E$=0.38 to the upper limit $1/k_P$=0.78 for N=0.1 and $1/k_P$=0.62 for N=0.3.

Finally, the effect of the ratio of hole diameter to specimen width D/W upon $\sigma^{net}_{max}/\sigma_0$ has been investigated for the choice α=2, σ_0/σ_y=3 and N=0.3; the predictions are shown in Fig. 14 for $0.1 \le D/W \le 0.8$. This choice of σ_0/σ_y is sufficiently large for the asymptotic tensile strength $\sigma^{net}_{max}/\sigma_0$ at large hole diameters to equal $1/k_P$. For all D/W the net section strength drops from $\sigma^{net}_{max}/\sigma_0$=1 to $\sigma^{net}_{max}/\sigma_0=1/k_P$ at a transition hole size $D/a_0 \approx 1$.

5. Concluding remarks

The plane strain, mode I crack growth resistance of metallic foams is modelled by a cohesive zone model embedded within a compressible elastic-plastic solid. The

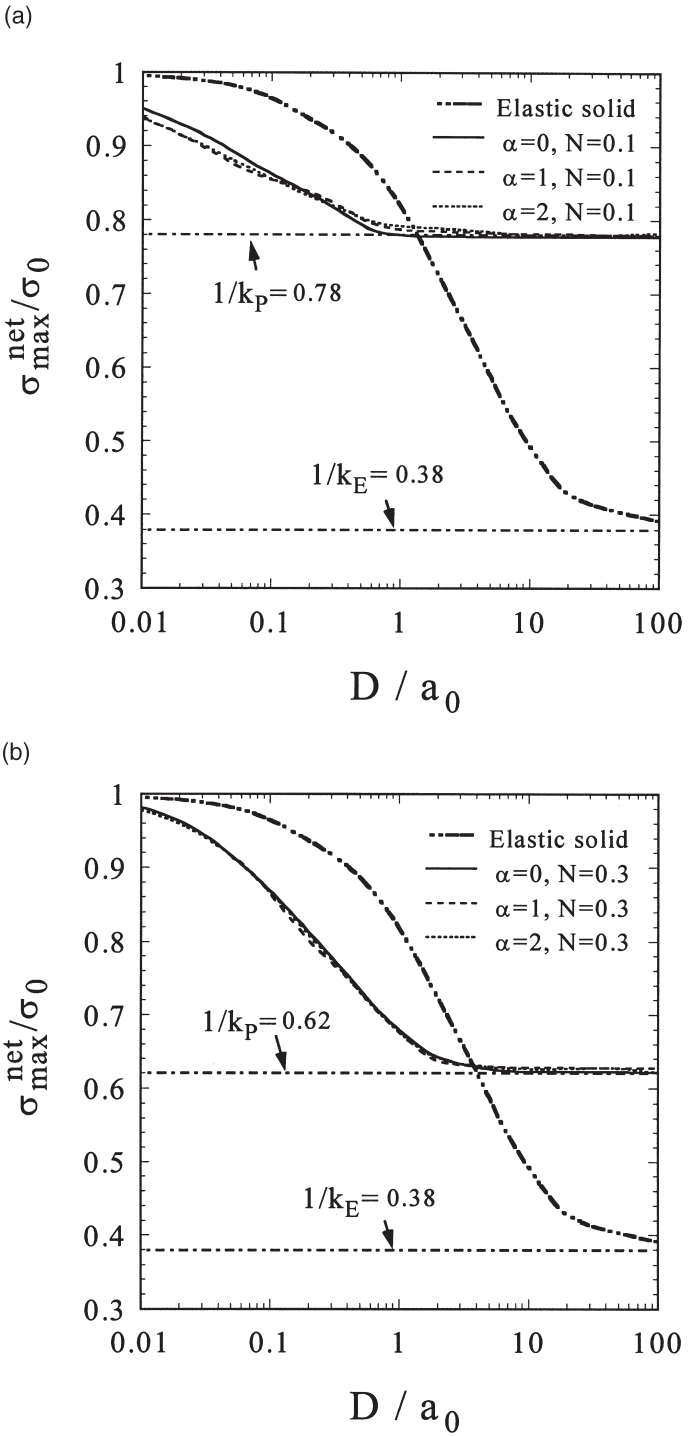

Fig. 13. Effect of the hole diameter upon the tensile strength of centre-hole specimen for the case D/W=0.1. (a) σ_0/σ_y=1.6 and N=0.1; (b) σ_0/σ_y=3 and N=0.3; (c) α=2 and N=0.1; and (d) α=2 and N=0.3.

(c)

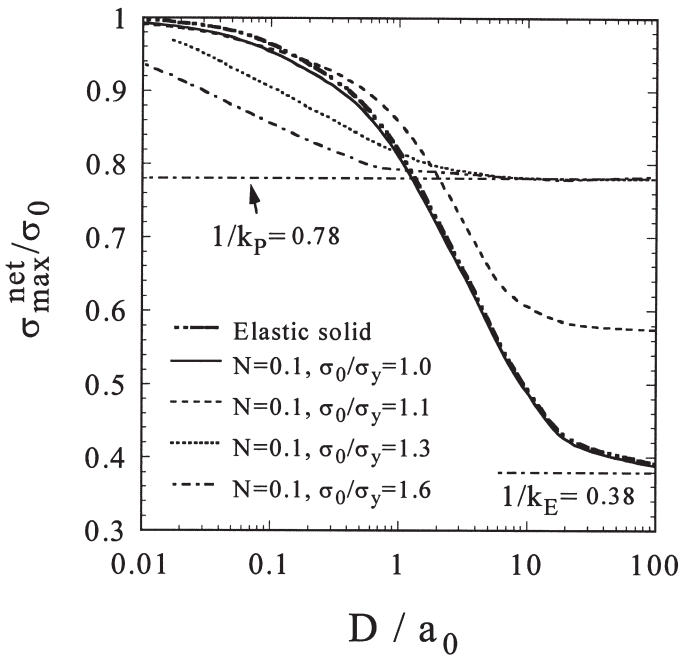

(d)

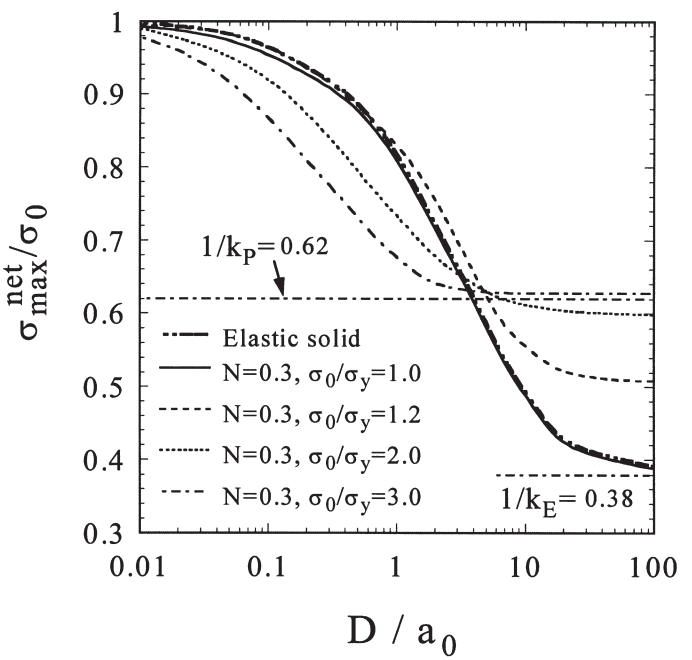

Fig. 13. (*continued*)

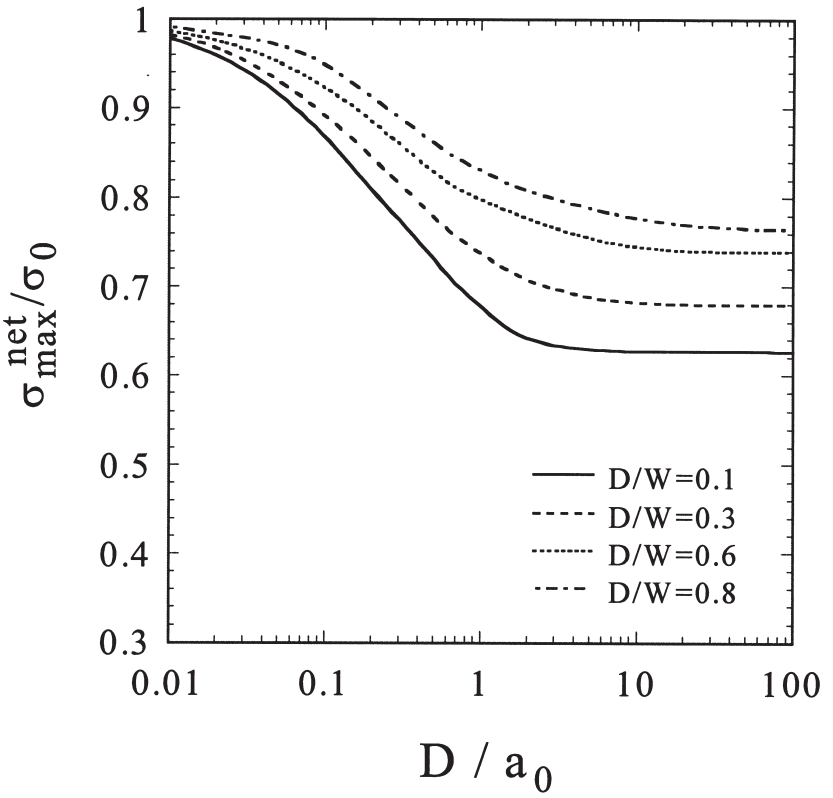

Fig. 14. Effect of the hole diameter upon the tensile strength of centre-hole specimen for selected values of D/W with α=2, σ_0/σ_y=3, and N=0.3.

effect of yield surface shape (as parameterised by the ratio of deviatoric strength to hydrostatic strength, α) upon the tearing resistance is explored. In general, an increase in α from the von Mises limit α=0 leads to a larger plastic zone ahead of the crack tip and to a higher crack growth resistance. It is found that the T-stress effect is significant only for nearly incompressible solids ($0\leq\alpha\leq1$), and is negligible for typical metallic foams (α=1~2). Consequently, we expect the measured toughness of metallic foams to be less sensitive to specimen geometry and loading configurations than that of fully dense metals.

The cohesive zone model has been used to determine the ductile-brittle transition for a panel containing a centre-hole or a centre-crack. For the case of a centre-crack, the behaviour switches from notch-insensitive at short crack length to an elastic-brittle response at long crack length: the transition crack size is $\alpha\approx\alpha_{SS}$. For the case of a panel containing an open hole of diameter D, the fracture response switches with increasing D from a net section strength criterion $\sigma^{net}_{max}\approx\sigma_0$ to a brittle behaviour $\sigma^{net}_{max}/\sigma_0=1/k$, where $k_P\leq k\leq k_E$. The transition hole size is given by $D\approx a_0$.

Acknowledgements

This work was supported by the EPSRC (U.K.) and by the DARPA/ONR (U.S.A.) MURI program on Ultralight Metallic Structures (No. N00014-1-96-1028). The authors are grateful for helpful discussions with Prof. M.F. Ashby.

References

ABAQUS Standard User's Manual, version 5.7, 1997. Hibbitt, Karlsson and Sorensen, Inc., Providence, Rhode Island.

Ashby, M.A., Evans, A.G., Fleck, N.A., Gibson, L.J., Hutchinson, J.W., Wadley, H.N.G., 2000. Metal Foams: a Design Guide. Butterworth Heinemann, Oxford.

Bao, G., Suo, Z., 1992. Remarks on crack-bridging concepts. Appl. Mech. Rev. 45, 355–366.

Bao, G., Zok, F., 1993. On the strength of ductile particle reinforced brittle matrix composite. Acta Mater. 41, 3515–3524.

Brezny, R., Green, D.J., 1989. Fracture behaviour of open cell ceramics. J. Am. Ceram. Soc. 72, 1145–1152.

Chen, C., 1998. Manual for a UMAT user subroutine. Technical Report CUED/C-MICROMECH/TR.4, Engineering Department, Cambridge University.

Chen, J.Y., Huang, Y., Oritz, M., 1998. Fracture analysis of cellular materials: a strain gradient model. J. Mech. Phy. Solids 46, 789–828.

Cottrell, A.H., 1963. Mechanics of Fracture, Tewksbury Symposium on Fracture, 1–27, University of Melbourne.

Deshpande, V.S., Fleck, N.A., 2000. Isotropic constitutive models for metallic foams. J. Mech. Phy. Solids 48, 1253–1283.

Du, Z.Z., Hancock, J.W., 1991. The effect of non-singular stresses on the crack tip constraints. J. Mech. Phy. Solids 39, 555–567.

Dugdale, D.S., 1960. Yielding of steel sheets containing slots. J. Mech. Phys. Solids 8, 100–104.

Fleck, N.A., Olurin, O.B., Chen, C., Ashby, M.F., 2001. The effect of hole size upon the strength of metallic and polymeric foams. J. Mech. Phys. Solids, to appear.

Gibson, L.J., Ashby, M.F., 1997. Cellular Solids: Structure and Properties, 2nd ed. Cambridge University Press, Cambridge.

Gibson, L.J., Ashby, M.F., Zhang, J., Triantafillou, T.C., 1989. Failure surfaces for cellular materials under multi-axial loads — I Modelling. Int. J. Mech. Sci. 31, 635–663.

Irwin, G.R., 1957. Analysis of stresses and strains near the end of a crack traversing a plate. ASME J. Appl. Mech. 24, 361–364.

Larsson, S.G., Carlsson, A.J., 1973. Influence of non-singular stress terms and specimen geometry on small scale yielding at crack tips in elastic-plastic materials. J. Mech. Phy. Solids 21, 263–277.

Maiti, S.K., Ashby, M.F., Gibson, L.J., 1984. Fracture toughness of cellular solids. Scripta Metall. 18, 213–217.

McCullough, K.Y.G., Fleck, N.A., Ashby, M.F., 1999a. Toughness of aluminium alloy foams. Acta Mater. 47, 2331–2343.

McCullough, K.Y.G., Fleck, N.A., Ashby, M.F., 1999b. Uniaxial stress-strain behaviour of aluminium alloy foams. Acta Mater. 47, 2323–2330.

Miller, R.E., 2000. A continuum plasticity model of the constitutive and indentation behaviour of foamed metals. Int. J. Mech. Sci. 42, 729–754.

Needleman, A., 1987. A continuum model for void nucleation by inclusion debonding. ASME J. Appl. Mech. 54, 525–531.

O'Dowd, N.P., Shih, C.F., 1991. Family of crack-tip fields characterised by a triaxiality parameter — I. Structure of fields. J. Mech. Phy. Solids 39, 989–1015.

Olurin, O.B., Fleck, N.A. and Ashby, M.F., 2001. Deformation and fracture of Aluminium foams. Mater. Sci. & Eng. A, to appear.

Rice, J.R., 1974. Limitations on the small scale yielding approximation for crack tip plasticity. J. Mech. Phy. Solids 22, 17–26.

Rice, J.R., Sorensen, E.P., 1978. Continuing crack-tip deformation and fracture for plane strain crack growth inelastic-plastic solids. J. Mech. Phy. Solids 26, 163–186.

Soutis, C., Fleck, N.A., Smith, P.A., 1991. Failure prediction technique for compression loaded Carbon Fiber-Epoxy Laminate with open hole. J. Composite Mater. 25, 1476–1498.

Sugimura, Y., Meyer, J., He, M.Y., Bart-Smith, H., Grenstedt, J., Evans, A.G., 1997. On the mechanical performance of closed cell Al alloy foams. Acta Mater. 45, 5245–5259.

Suo, Z., Bao, G., Fan, B., 1992. Delamination R-curves due to damage. J. Mech. Phys. Solids 40, 1–16.

Suo, Z., Ho, S., Gong, X., 1993a. Notch ductile-to-brittle transition due to localised inelastic band. ASME J. Eng. Mater. Tech. 115, 319–326.

Suo, Z., Shih, C., Varias, A.G., 1993b. A theory for cleavage cracking in the presence of plastic flow. Acta Mater. 41, 1551–1557.

Tada, H., Paris, P.C., Irwin, G.R., 1985. The Stress Analysis of Cracks Handbook. Del Research, St. Louis, MO.

Tvergaard, V., Hutchinson, J.W., 1992. The relation between crack growth resistance and fracture process parameters in elastic-plastic solids. J. Mech. Phy. Solids 40, 1377–1397.

Tvergaard, V., Hutchinson, J.W., 1994. Effect of T-stress on mode-I crack growth resistance in a ductile solid. Int. J. Solids & Struct. 31, 823–833.

Yuan, H., Brocks, W., 1998. Quantification of constraint effects in elastic-plastic crack front fields. J. Mech. Phy. Solids 46, 219–241.

Zhang, J., Lin, Z., Wong, A., Kikuchi, N., Li, V.C., Yee, A.F., Nusholtz, G.S., 1997. Constitutive modelling and material characterisation of polymeric foams. ASME J. Eng. Mater. Tech. 119, 284–291.